scientific reports

Check for updates

OPEN

Optimization of photochemical decomposition of aniline in aqueous solutions and assessment of effluent toxicity using *Pseudomonas aeruginosa ATCC 27853*

Mansour Ghaderpoori[1], Maryam Hossini[2], Faramarz Azimi[1], Bahram Kamarehie[1] & Ali Toolabi[1]✉

Aniline is a toxic chemical compound that poses serious risks to human health. Its introduction into aquatic environments can threaten the health of humans and other living organisms. This study aimed to investigate the removal of aniline from aqueous solutions using the TiO_2/H_2O_2/UV photocatalytic process and to evaluate the toxicity of the treated effluent. Experiments were conducted under controlled laboratory conditions using a photocatalytic batch reactor with an approximate volume of three liters. To investigate the effects of pH, TiO_2 nanoparticle concentration, initial concentration, and contact time on aniline removal efficiency, a Central Composite Design (CCD) was employed. Data analysis was carried out using Design Expert software, version 13. In addition, the toxicity of the effluent was assessed using the Alamar Blue (AB) reduction assay, which is based on the metabolic activity of *Pseudomonas aeruginosa*. The results of this study showed that the maximum aniline removal efficiency under optimized conditions reached 98%. Furthermore, the toxicity of the treated effluent was assessed using a novel evaluation method based on the AB assay and the metabolic activity of *P. aeruginosa*. Based on this assessment, the EC_{50} value was determined to be 1.64 mg/L. A significant correlation was observed between the reduction of AB dye and the viability of *P. aeruginosa*, confirming the reliability of this method for post-treatment toxicity monitoring. The findings of this study demonstrated that the photocatalytic process exhibited a reasonable efficiency in degrading aniline and was, also, capable of reducing the biological toxicity of the treated effluent. Accordingly, when combined with the novel toxicity assessment method introduced in this study, this process may be considered a viable option for enhancing advanced industrial wastewater treatment.

Keywords Aniline decomposition, Titanium dioxide nanoparticles, Alamar blue, Effluent toxicity

Abbreviations

CCD	Central Composite Design
AB	Alamar Blue
EC_{50}	Median Effective Concentration
NOEC	No Observed Effect Concentration
AOPs	Advanced Oxidation Processes
SBR	Sequencing Batch Reactor
LET	Linear Energy Transfer
RSM	Response Surface Methodology
SEM	Scanning Electron Microscopy
EDX	Energy Dispersive X-ray Spectroscopy

[1]Environmental Health Research Center, Lorestan University of Medical Sciences, Khorramabad, Iran. [2]Student Research Committee, Lorestan University of Medical Sciences, Khorramabad, Iran. ✉email: atoolabi@yahoo.com

3D	Three-Dimensional
ANOVA	Analysis of variance
ROS	Reactive Oxygen Species
IEP	Isoelectric Point

Environmental pollution is one of the major global problems. These pollutions primarily result from the discharge of industrial waste, chemical fertilizers, pharmaceutical waste, household waste, and pesticides[1,2]. Currently, the ecological environment and human health are threatened by the increasing levels of organic pollutants in water[3]. Since the beginning of the new century, more than half a million organic compounds have been synthesized, with approximately 1,000 new organic compounds being created each year[4].

Aniline is considered one of the most hazardous organic compounds due to its toxic effects on both human health and the environment[5]. It is a carcinogenic substance[6] widely used in textiles, oil, rubber, pharmaceuticals, herbicides[7], explosive stabilizers, plastic modifiers[8], vulcanization accelerators, pesticides, and disinfectants[9]. When this toxic substance enters the bloodstream, it interferes with oxygen absorption by converting hemoglobin into ethemoglobin, leading to a condition known as methemoglobinemia. Furthermore, this substance induces hemolytic damage to red blood cells, leads to anemia, adversely affects splenic function, promotes oncogenic tumor formation, and significantly elevates the risk of bladder cancer in humans[10,11]. The International Agency for Research on Cancer (IARC) has classified aniline as a Group 2B carcinogen, indicating that it is possibly carcinogenic to humans due to its mutagenic and carcinogenic potential[12]. Therefore, aniline must be removed before discharging effluents into the around environment. Various treatment methods have been explored for the removal of aniline from aqueous solutions, including coagulation-flocculation[5,9], remedial technologies[10], magnetic catalysts[13], electro-polymerization methods[14], UV/proxy disulfate processes[15], electrochemical treatments[16], and photocatalytic oxidation processes[17].

Recently, Advanced Oxidation Processes (AOPs) have demonstrated strong oxidative capabilities, effectively degrading persistent pollutants such as aniline. These processes typically generate reactive species, including hydroxyl radicals (•OH) and superoxide radicals ($O_2^{\bullet-}$), through various combinations of hydrogen peroxide, ozone, nanoparticles, and ultraviolet irradiation. Recognized as emerging technologies, AOPs are widely employed as heterogeneous photocatalysts for the degradation of environmental pollutants[18,19]. Among these, heterogeneous photocatalytic oxidation using TiO_2 nanoparticles, hydrogen peroxide, and UV irradiation has been introduced as an effective method for degrading resistant pollutants[20,21]. As shown in Eq. 1, when H_2O_2 absorbs UV light, •OH are generated:

$$H_2O_2 + h\nu \rightarrow 2\,^{\bullet}OH \tag{1}$$

Hydrogen peroxide serves as the primary source of hydroxyl radical (•OH) generation. Additionally, •OH radicals can also form in aqueous media when water molecules are oxidized by the catalyst. The generation rate of these radicals is influenced by the linear energy transfer (LET) and the pH of the solution. The formation of the resulting products follows the reaction presented in Eq. 2[18].

$$H_2O \rightarrow {}^{\bullet}OH\ (2.8), {}^{\bullet}H\ (0.6), e^-\ (2.7), H_2\ (0.45),\ H_2O_2\ (0.72),\ H^+\ (3.2), OH^-\ (0.5) \tag{2}$$

Although the TiO_2/UV process is widely employed for the oxidation of organic compounds in wastewater, it is particularly effective in degrading pollutants with complex molecular structures, such as aniline[19]. A study conducted by Jia et al. demonstrated that catalytic processes were capable of removing up to 93.5% of aniline from aqueous solutions[13]. In another study, Maybahi et al. investigated the photocatalytic effect of nanoparticles on the degradation rate of aniline. Their results demonstrated that, under optimal experimental conditions—including pH, pH, contact time, and nanoparticle dosage the aniline removal efficiency reached 78.1%[22]. Moreover, Yablack et al. conducted a comprehensive evaluation of aniline oxidation using hydrogen peroxide, demonstrating that this method is highly efficient for aniline removal, Their results indicated a maximum removal efficiency of 99.21%, highlighting the significant potential of hydrogen peroxide as an oxidizing agent in wastewater treatment processes[23].

Although AOPs are known for their efficiency in removing persistent organic contaminants from water solutions, the generation of potentially harmful intermediates or transformation products remains a notable concern. AOPs rely on the generation of reactive radicals, particularly •OH, to break down organic pollutants. However, the degradation pathways can sometimes lead to the formation of intermediate compounds with residual or unknown toxicity. Therefore, performing a thorough toxicity evaluation of the effluents produced by such systems is necessary to verify their environmental safety and treatment effectiveness.

To address this, biological assays are increasingly used as complementary tools to chemical analysis. Among them, the alamar blue (AB) assay method has gained recognition due to its ability to detect changes in cellular metabolic activity through a measurable color change. This technique stands out for being highly sensitive, non-toxic to cells, easy to perform, rapid and economically feasible[24–26]. Its application in environmental toxicology allows for early identification of harmful effects that might not be captured through conventional analytical methods. Thus, integrating such bioassays into effluent evaluation protocols provides a more comprehensive assessment of the ecological risks associated with treated wastewater[25,27]. This method assesses the activity of the electron transport system (ETS) dehydrogenase enzyme, which is directly correlated with the amount of oxygen consumed. Under these conditions, AB dye is reduced to resorufin by the bacterial electron transport system, enabling quantification of bacterial metabolic activity[18,19].

In a study, Zare et al. evaluated the toxicity of effluent from a Sequencing Batch Reactor (SBR) using the AB assay. Their findings showed that the AB dye was reduced by metabolically active bacteria present in the

wastewater, and the extent of this reduction-indicated by a measurable color change-was used to quantify bacterial activity[25].

Additionally, Toolabi et al. demonstrated the effectiveness of the AB assay in determining the toxicity of effluents from photocatalytic reactors. In their study, *P. aeruginosa* was employed as the test microorganism due to its high sensitivity to toxic substances commonly present in effluent. The reduction of AB by metabolically active bacteria enabled reliable quantification of bacterial viability, establishing this method as a valuable tool for toxicity assessment in wastewater treatment processes. Furthermore, their findings confirmed that AB serves as a rapid, sensitive, and cost-effective indicator for evaluating the biological effects of treated effluents[28]. To date, no study has investigated the toxicity of aqueous solutions treated via a photocatalytic process for aniline removal using the AB assay to quantify the activity of reductive dehydrogenase enzymes in *P. aeruginosa*. Accordingly, the present study aimed to eliminate aniline from aqueous solutions through a TiO_2/H_2O_2/UV-based photocatalytic process and to assess the toxicity of the treated effluent by evaluating the metabolic activity of *P. aeruginosa* ATCC 27853.

Materials and methods

Preparation of materials

Hydrogen peroxide, sodium hydroxide, hydrochloric acid, and aniline (99.5% purity) were purchased from Merck, Germany. Titanium dioxide was supplied by Pishgaman Nano Materials Company, Mashhad, Iran. Nutrient broth, KH_2PO_4, K_2HPO_4, glucose, sodium acetate, dimethyl sulfoxide, n-amyl alcohol, and sodium bicarbonate were available in our laboratory. The chemical and physical properties of aniline are summarized in Table 1.

Microorganism

To biologically assess the toxicity of the effluent, a standard strain of *P. aeruginosa* ATCC 27853 was obtained from the Tehran Razi Institute. Subsequently, a bacterial suspension was prepared according to the 0.5 McFarland standard. The 0.5 McFarland standard was employed as a turbidity reference to standardize the concentration of bacterial suspensions prior to antibiotic susceptibility testing. This standard was prepared by forming a barium sulfate ($BaSO_4$) precipitate through the reaction of 0.5 mL of barium chloride with 99.50 mL of diluted sulfuric acid. The turbidity of the resulting suspension was verified Spectrophotometry at a wavelength of 625 nm, with absorbance values ranging between 0.08 and 0.12. To ensure consistency and reproducibility in microbial assays, the final suspension was adjusted to match a bacterial density of approximately 1.5×10^8 colony-forming units per milliliter (CFU/mL)[29,30].

Modeling and statistical analysis

In this study, Response Surface Methodology (RSM) was employed to optimize the experimental data. RSM is an advanced statistical technique used for modeling, analyzing, and optimizing complex processes with multiple variables. This algorithm models the relationship between input and output variables to identify the optimal conditions for the process. Data analysis was conducted using Design-Expert software, version 13.

The Central Composite Design (CCD), one of the most commonly used designs in RSM, was employed in this study. CCD model enables the development of an accurate model of the system response while minimizing the number of required experiments. In the CCD model, experimental points include center points that help determine repeatability and experimental error. This design is particularly suitable for exploring quadratic response surfaces and efficiently estimating interactions among variables[31,32]. The quadratic model is mathematically represented by the following equation (Eq. 3):

$$Y = \beta_0 + \sum_{i=1}^{k} \beta_i x_i + \sum_{i=1}^{k} \beta_{ii} x_i^2 + \sum_{1 \le i \le j}^{k} \beta_{ij} x_i x_j \quad (3)$$

Where:

Y = predicted response.
β0 = constant coefficient.
βi = linear regression coefficients.
βii = quadratic coefficients.

Category	Detail
Formula	$C_6H_5NH_2$
Structure	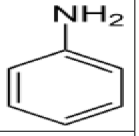
Molar mass (g/mole)	93.13
Density g/cm³	1.02
Solubility in water (g/L at 20 °C)	36

Table 1. Physical and chemical properties of Aniline.

Factor	Parameter Level			
	Code	1-	0	1+
Contact time (min)	A	15	67.50	120
pH	B	3	7.50	12
Concentration of aniline(mg/L)	C	1	20.50	40
Dose of NPs (mg/L)	D	10	55	100

Table 2. The levels of variables central composite statistical experiment design.

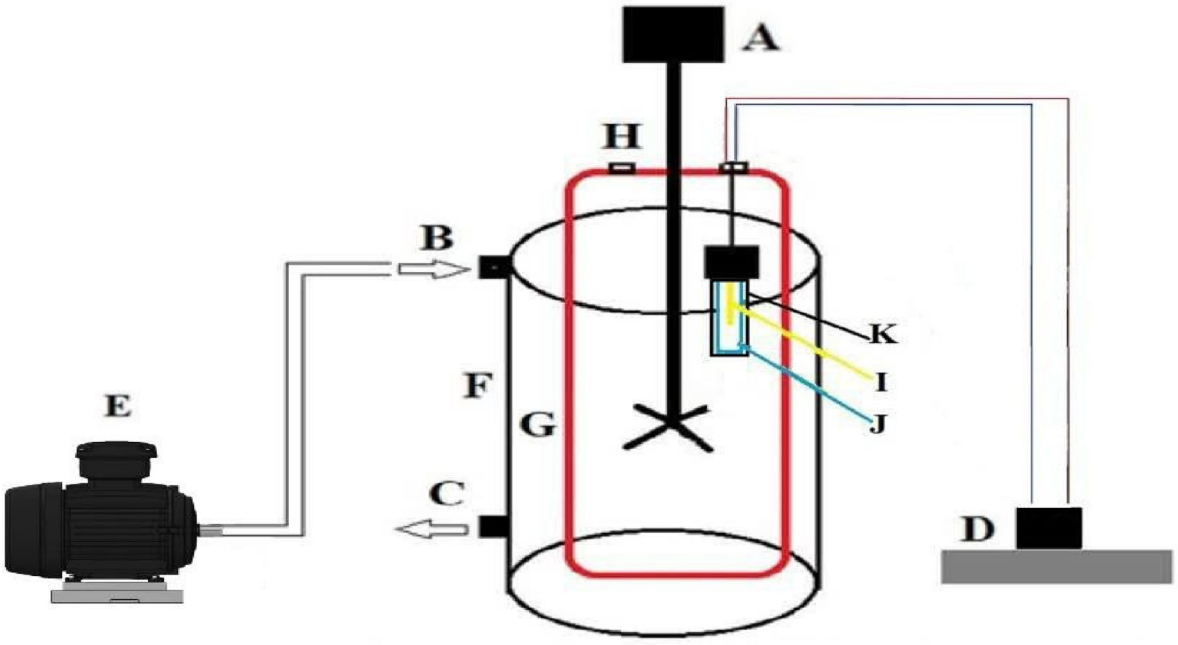

Fig. 1. Schematic representation of a photocatalytic reactor system (A = mechanical mixer, B = water inlet, C = water outlet, D = Source of electricity, E = pump, F = Cooling system, G = photocatalytic reactor, H = Sampling point, I = UV lamp, J = Quartz sleeve, K = Cut off filter).

βij = interaction coefficients.

Xj and Xj = coded values of the independent variables.

In the present study, the number of experimental runs was determined based on the CCD model, considering key variables such as aniline concentration (1–40 mg/L), contact time (15–120 min), pH (3–12), and nanoparticle dose (10–100 mg/L), as summarized in Table 2. The ranges of these variables were determined based on several factors, including preliminary tests, results from previous studies, and environmental regulations pertaining to the discharge of aniline-containing wastewater.

Photocatalytic experiments

Photocatalytic experiments were performed under conditions determined by the CCD model, using a photoreactor with an approximate volume of three liters (Fig. 1). The reactor was equipped with a UV lamp (P = 125 W, L = 12 cm) emitting light in the 251–257 nm range, with a peak emission at λ_{max} = 254 nm. To prevent exposure to external UV radiation, the walls of the photoreactor were lined with aluminum foil. To enhance the efficiency of the photochemical process in removing aniline, hydrogen peroxide was added at a concentration of 50 mg/L. A magnetic stirrer was employed inside the reactor to uniform dispersion and mix the nanoparticles. After the reaction, the samples were centrifuged at 2000 rpm for 1 min to separate and settle the nanoparticles. Aeration was provided using a pump at a flow rate of 1.5 L/min to enhance aniline oxidation and facilitate the generation of hydroxyl radicals. The pH of the solution was adjusted using 0.1 M sodium hydroxide and 0.1 M hydrochloric acid.

Finally, the residual concentration of aniline was measured using a UV/Vis spectrophotometer (HACH-Lange DR 5000, USA) at a wavelength of λmax = 235 nm. The percentage of aniline removal was calculated using Eq. 4.

$$\text{Removal efficiency } \% = \frac{(C_0 - Ce) \times 100}{C_0} \quad (4)$$

Where:

C_0 = Initial concentration of aniline (mg/L).
C_e = Residual aniline concentration after the experiments (mg/L).

Effluent toxicity assessment

In this study, bacterial mortality or inactivation of *P. aeruginosa* was assessed by measuring the percentage of bacterial growth inhibition following the photocatalytic process. To this end, the reduction of the AB dye by *P. aeruginosa* was evaluated. The rate of AB dye reduction, mediated by the dehydrogenase enzyme of *P. aeruginosa*, was determined using the following procedure[25,28,31].

Firstly, the nutrient broth culture medium (1.6 g/L) was supplemented with KH_2PO_4 (1.64 g/L), K_2HPO_4 (2.64 g/L), glucose (0.2 g/L), and sodium acetate (0.2 g/L). Subsequently, 2.25 mL of dimethyl sulfoxide, 1 mL of bacterial suspension, and 1 mL of AB solution (100 g/L) were added to the medium. After a contact time of 30 min, 10 mL of n-amyl alcohol solution and 1 mL of 0.5 M HCl-phthalate buffer were added to each test tube. The samples were then centrifuged at 1000 g for 5 min. After centrifugation, the supernatant alcohol layer was transferred to a microplate well containing 2 g of sodium bicarbonate. Finally, the absorbance of the AB dye was measured at 610 nm using a spectrophotometer. A control sample without bacteria was prepared simultaneously for comparison. In the presence of *P. aeruginosa*, the activity of the dehydrogenase enzyme reduces AB to resorufin, causing the solution's color to change from blue to pink. Therefore, this dye change serves as an indicator of the metabolic activity of *P. aeruginosa*. Based on Eq. 5, the percentage of reduction in the growth of *P. aeruginosa* was calculated. The results were reported in terms of effective concentrations (EC), 100% mortality, and no observed effect concentrations (NOEC).

$$\begin{aligned}&\text{Reduction of dehydrogenase enzyme activity}, \% = (\text{A-B}) \ /\text{A} \times 100\\&\text{A: Dehydrogenase enzyme activity in the control sample}\\&\text{B: Dehydrogenase enzyme activity in the original sample}\end{aligned} \tag{5}$$

Results

Scanning electron microscopy and energy dispersive X-ray spectroscopy analysis

The results of the SEM analysis of titanium dioxide are shown in Fig. 2a. The image clearly shows the relatively spherical shape of the particles with a uniform size distribution. Also, dimensional measurements based on SEM showed that the average particle size was in the range of 13 to 22 nm. To evaluate the elemental composition of the sample, energy dispersive X-ray spectroscopy (EDX) analysis was performed on the surface of the nanoparticles (Fig. 2b). The results indicated that titanium (Ti) and oxygen (O) were the main elements present. The weight percentages (W%) and atomic percentages (A%) of these elements were determined as 52.7% and 27.12% for titanium, and 47.3% and 72.88% for oxygen, respectively.

Modeling and statistical analysis

In this study, RSM combined with CCD was employed to optimize the removal of aniline from aqueous solutions using a titanium dioxide nanophotocatalyst. The maximum removal efficiency of aniline (98%) was achieved under the following conditions: an initial aniline concentration of 1 mg/L, nanophotocatalyst dosage of 55 mg/L,

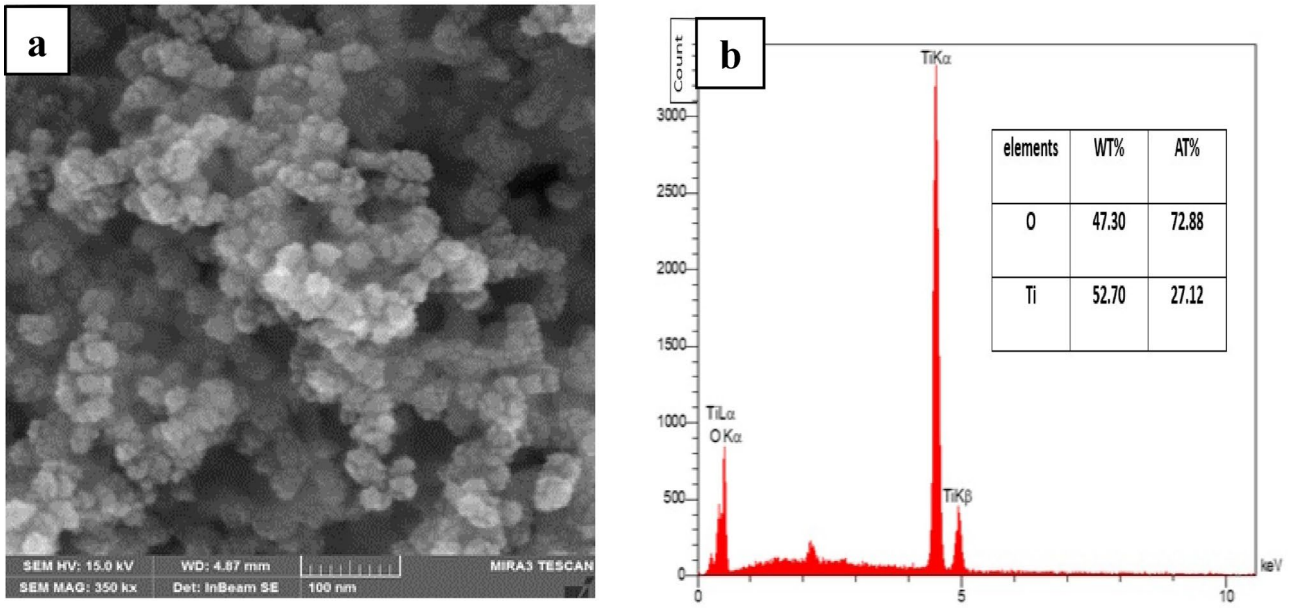

Fig. 2. **(a)** SEM and **(b)** EDX spectrum of TiO_2 nanoparticles.

Run order	Factor A (min)	Factor B	Factor C (mg/L)	Factor D (mg/L)	Removal efficiency %	Predicted RE, %
1	62.50	7.50	20.50	55.00	90.60	90.15
2	36.25	5.25	30.25	32.50	84.00	83.98
3	36.25	9.75	10.75	77.50	91.00	90.69
4	62.5	7.50	20.50	55.00	90.00	90.15
5	88.75	5.25	10.75	77.50	91.50	91.28
6	88.75	5.25	30.25	32.50	83.70	84.29
7	88.75	5.25	30.25	77.50	85.50	84.95
8	88.75	9.75	30.25	77.50	86.60	86.17
9	36.25	5.25	10.75	77.50	91.00	90.76
10	88.75	5.25	10.75	32.50	90.50	90.40
11	62.50	7.50	20.50	55.00	90.80	90.15
12	88.75	9.75	30.25	32.50	85.50	85.45
13	36.25	5.25	30.25	77.50	84.00	84.11
14	36.25	9.75	30.25	77.50	84.00	83.81
15	36.25	5.25	10.75	32.50	89.70	90.41
16	36.25	9.75	10.75	32.50	90.00	90.26
17	88.75	9.75	10.75	77.50	93.00	92.73
18	88.75	9.75	10.75	32.50	91.60	91.77
19	36.25	9.75	30.25	32.50	83.10	83.61
20	62.50	12.00	20.50	55.00	78.30	78.45
21	62.50	7.50	40.00	55.00	85.00	85.01
22	115.00	7.50	20.50	55.00	92.00	92.43
23	62.50	3.00	20.50	55.00	77.50	77.36
24	62.50	7.50	20.50	55.00	90.20	90.15
25	62.50	7.50	20.50	100.00	90.00	91.05
26	62.50	7.50	1.00	55.00	98.00	98.00
27	10.00	7.50	20.50	55.00	90.50	90.08
28	62.50	7.50	20.50	55.00	90.20	90.15
29	62.50	7.50	20.50	55.00	89.10	90.15
30	62.50	7.50	20.50	10.00	91.00	89.96

Table 3. Results obtained from the design of experiments in the photocatalytic removal of aniline.

Source	Dev.	*R*-Squared	Adjusted *R*-Squared	Predicted *R*-Squared	Press	Summary
Linear	3.45	0.4707	0.3860	0.1931	453.71	-
2FI	3.94	0.4757	0.1997	0.1616	471.41	-
Quadratic	0.65	0.9887	0.9781	0.9483	29.06	Suggested
Cubic	0.55	0.9963	0.9846	0.9108	50.17	Aliased

Table 4. Model summary statistics and standard Deviation.

pH of 7.5, and a contact time of 62.5 min (Table 3). In contrast, the minimum removal efficiency (77.5%) was observed in run number 23, corresponding to an initial aniline concentration of 20.5 mg/L, nanophotocatalyst dosage of 55 mg/L, pH of 3, and a similar contact time. Based on CCD results, four different regression models were proposed. The statistical findings are presented in Table 4. According to Table 4, the quadratic model was selected as the most appropriate for aniline removal, with a coefficient of determination (R^2) of 0.9887, an adjusted coefficient of determination ($_{R^2\ adjusted}$) of 0.9781, and a predicted coefficient of determination ($R^2_{predicted}$) of 0.9386.

In this study, the results of the quadratic model analysis of variance indicated that (Table 5). The initial aniline concentration and pH had significant effects on the photocatalytic removal of aniline (P-value < 0.05), whereas the nanoparticle dose and contact time did not show statistically significant effects (P-value > 0.05). The model yielded an F-value of 93.64 with 14 degrees of freedom, indicating a high level of statistical validity and a good fit to the experimental data.

Source	Sum of Square	df	Mean Square	F Value	*p*-value	Prob > F
Model	555.95	14	39.71	93.64	< 0.0001	significant
A	4.43	1	4.43	10.45	0.1936	
B	0.79	1	0.79	1.85	< 0.0001	
C	95.52	1	95.52	225.26	< 0.0001	
D	0.27	1	0.27	0.63	0.4396	
AB	2.33	1	2.33	5.48	0.0334	
AC	0.11	1	0.11	0.25	0.6250	
AD	0.28	1	0.28	0.65	0.4327	
BC	0.051	1	0.051	0.12	0.7345	
BD	5.625E-003	1	5.625E-003	0.013	0.9098	
CD	0.051	1	0.051	0.12	0.7345	
A^2	2.09	1	2.09	4.93	0.0422	
B^2	257.08	1	257.08	606.23	< 0.0001	
C^2	3.14	1	3.14	7.41	0.0157	
D2	0.22	1	0.22	0.51	0.4873	
Residual	6.36	15	0.42			
Lack of Fit	4.61	10	0.46	1.31	0.4029	
Pure Error	1.75	5	0.35			not significant
Cor Total	562.31	29				

Table 5. ANOVA for response surface quadratic Model.

According to the quadratic regression equation, the empirical relationship between the parameters and aniline removal efficiency is expressed by Eq. 6:

$$\begin{aligned}\text{Removal efficiency}, \% = {} & +67.25116 - (0.094837 \times \text{Time}) + (8.82011 \times \text{pH}) - (0.46543 \times \text{C}) \\ & - (0.018612 \times D) + (6.45503 \times Time \times pH) + (3.17460 \times Time \times C) \\ & + (2.22222 \times Time \times D) - (2.56410 \times pH \times C) + (3.70370 \times pH \times D) \\ & - (2.56410 \times C \times D) + (4.00605 \times Time^2) - (0.60473 \times p\text{H}^2) \\ & + (3.56125 \times \text{C}^2) + (1.74897 \times \text{D}^2)\end{aligned} \quad (6)$$

After extracting the second-order regression model, the predicted values were calculated by substituting the data into the model equation, and the residuals were determined as the differences between the actual and predicted values. Based on the results shown in Fig. 3a, the normal probability plot of the residuals follows a normal distribution, with no significant systematic errors observed. Additionally, the predicted values were in good agreement with the actual values, indicating the adequacy and high accuracy of the model in prediction Fig. 3b.

The effects of parameters on aniline removal

After identifying the role of individual parameters on the response variable, the interactions between factors should be examined. Based on the results obtained, only the interaction between contact time and pH on the aniline removal process was statistically significant. Figure 4 presents a three-dimensional (3D) plot of removal efficiency as a function of pH and contact time. Accordingly, as the pH increases from 3 to 7.5 and the contact time from 10 to 62.5 min, the removal efficiency rises from 77.5% to 98% (Fig. 4a). Furthermore, an increase in pH beyond 7.5 and contact time longer than 62.5 min results in a decrease in removal efficiency.

Therefore, the aniline removal process was conducted at a pH of approximately 7.5 and a contact time of 62.5 min. Figure 4b presents a 3D plot of aniline removal efficiency as a function of the interaction between contact time and initial aniline concentration. It was observed that the highest removal efficiency was achieved at an aniline concentration of 1 mg/L with a contact time of 62.5 min. Furthermore, increasing both the initial aniline concentration and contact time led to a decrease in the removal efficiency. Figure 4c illustrates a 3D plot of removal efficiency as a function of contact time and nanoparticle dosage. It was observed that the highest removal efficiency occurred at a contact time of 62.5 min and a titanium dioxide nanoparticle dose of 55 mg/L. Moreover, further increases in both contact time and nanoparticle dosage at higher concentrations resulted in a decrease in aniline removal efficiency. In this study, the interaction effects between pH and initial aniline concentration on removal efficiency were also investigated.

According to Fig. 4d, the highest aniline removal efficiency of 98% was achieved at an initial concentration of 1 mg/L and a pH of approximately 7.5. As both pH and initial aniline concentration increased, the removal efficiency decreased to 85%. Based on Table 3, Run order 26, the highest removal efficiency under optimal variable conditions was reported as 98%. An increase in pH and nanoparticle dosage (Fig. 4e) also resulted in a decline in aniline removal efficiency. By studying the interaction between nanoparticle dose and initial aniline concentration (Fig. 4f), it was determined that the removal efficiency reached 98% at an initial concentration of 1 mg/L and a nanoparticle dose of 55 mg/L. In other words, removal efficiency increased at low aniline

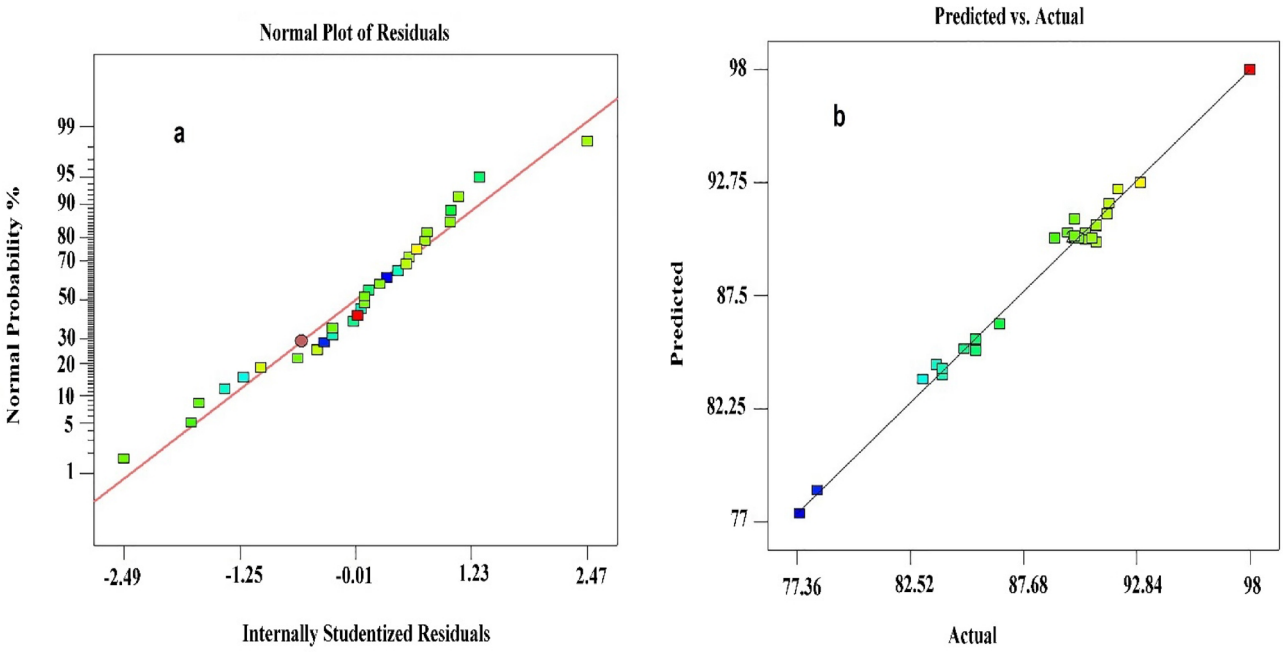

Fig. 3. **(a)** Probability plot of the residual distribution, **(b)** actual values versus predicted values.

concentrations and optimal nanoparticle dosages. Further details of the experimental results are presented in Fig. 4; Table 3.

Alamar blue toxicity assessment

In this study, following the photocatalytic process conducted according to the number of designed runs, toxicity analysis was performed using the AB reduction assay on *P. aeruginosa* bacteria. The results obtained are presented in Table 6. Accordingly, the EC_{50}, NOEC, and 100% mortality values were reported as 1.64, 0.91, and 1.97 mg/L, respectively. Detailed information and additional data are presented in Table 6.

Discussion

In this study, scanning electron microscopy (SEM) and energy-dispersive X-ray spectroscopy (EDX) analyses were performed to investigate the surface morphology and chemical composition of titanium dioxide nanoparticles (Fig. 2). SEM results revealed that the nanoparticles were aggregated into clusters exhibiting a relatively uniform distribution and predominantly spherical morphology on the catalyst surface. This structural arrangement contributed to the enhancement of the material's physicochemical uniformity. Furthermore, the particle sizes were within the nano scale range (i.e., less than 100 nm) (Fig. 2a), confirming the nanostructured nature of the catalyst. This feature is significant because the properties of nanoparticles typically improve substantially within this size range. Moreover, the presence of small pores on the catalyst surface may play a crucial role in enhancing adsorption processes and photocatalytic reactions by increasing the accessible active surface area. Such a porous structure likely contributes to the improved efficiency of pollutant degradation, which is particularly important for environmental and industrial applications. Therefore, the SEM results not only confirm the morphological characteristics of the nanoparticles but also facilitate a better understanding of the catalyst's performance in photocatalytic processes, providing a solid foundation for further optimization of the material's properties[20,28]. In this study, energy-dispersive X-ray spectroscopy (EDX) analysis was performed to determine the elemental composition of the synthesized titanium dioxide nanoparticles, as illustrated in Fig. 2b. The results confirmed the successful synthesis of TiO_2 nanoparticles with a titanium-to-oxygen atomic ratio close to the ideal stoichiometric value of 1:2. Maintaining this stoichiometric accuracy is crucial, as deviations—such as oxygen vacancies—can significantly affect the electronic structure and photocatalytic performance of TiO_2[33]. Furthermore, the absence of detectable impurities in the EDX spectrum indicated that the sample possessed high chemical purity, which contributed to the reduction of surface defects and recombination centers. The high-purity TiO_2 nanoparticles with precisely controlled composition exhibited enhanced photocatalytic activity, attributed to improved charge separation and reduced electron–hole recombination. These findings are consistent with previous reports and validate the effectiveness of the employed synthesis method[21,34,35]. For more comprehensive structural and electronic characterization of the synthesized nanoparticles, the use of complementary techniques such as X-ray photoelectron spectroscopy (XPS) and X-ray diffraction (XRD) is recommended for future studies.

In this study, the application of RSM combined with CCD model was employed as an effective approach for optimizing the aniline removal process (Table 3). In addition to demonstrating strong statistical validity, evidenced by a high coefficient of determination, the findings highlighted several advantages of CCD beyond mere modeling, including a reduction in the number of experimental runs and enhanced predictive accuracy

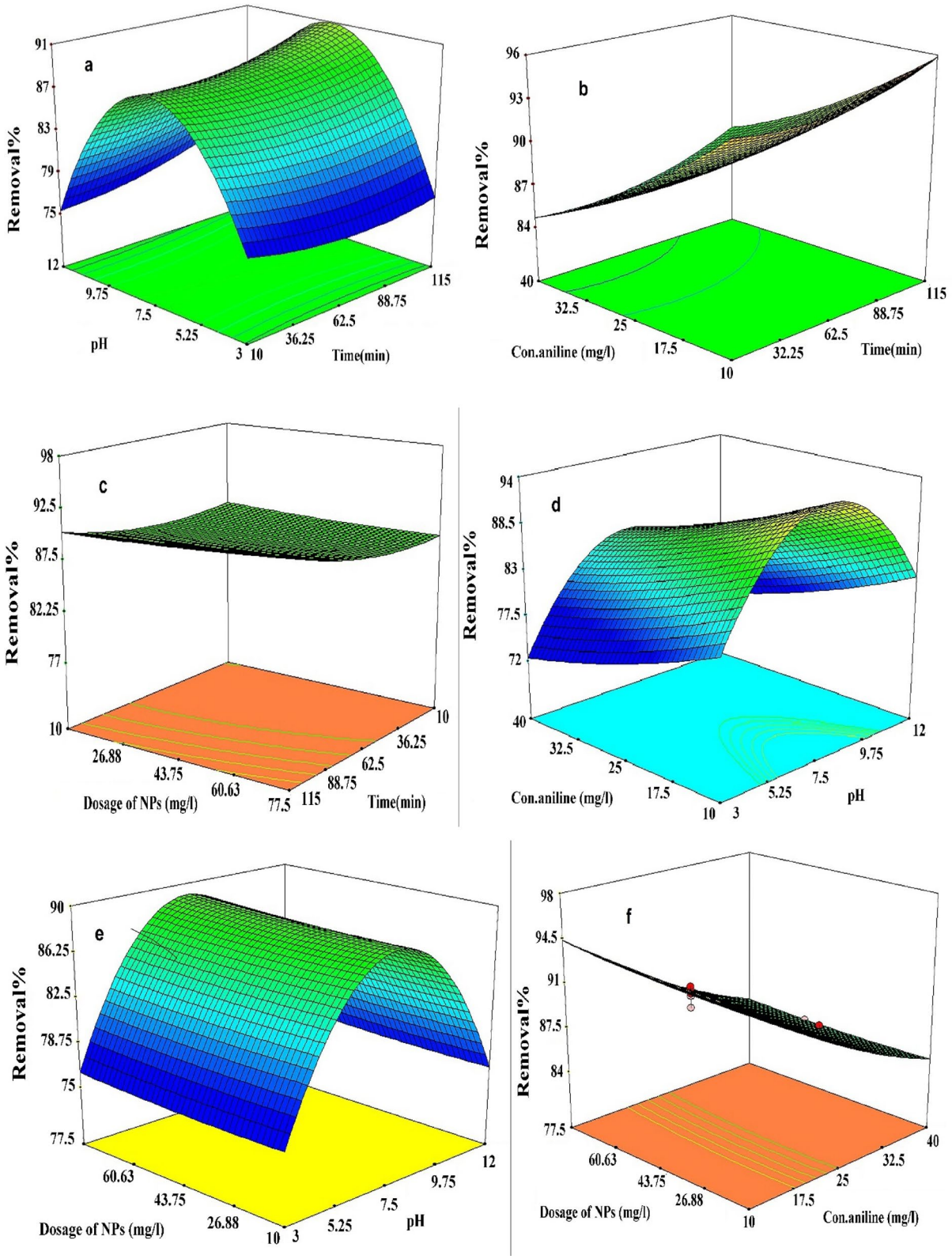

Fig. 4. 3D model response for aniline removal with interaction between factors: contact time (min), pH, nanoparticle dose (mg/L) and aniline concentration (mg/L).

Run order	Aniline concentration in the reactor effluent (mg/L)	The rate of reduction in the activity of *P. aeruginosa* bacteria based on the AB reduction
1	1.92	EC_{90}
2	5.14	100% mortality
3	0.96	EC_{10}
4	2.05	EC_{100}
5	0.91	NOEC
6	4.93	100% mortality
7	4.38	100% mortality
8	4.05	100% mortality
9	0.96	EC_{11}
10	1.02	EC_{60}
11	1.88	EC_{60}
12	4.71	100% mortality
13	4.84	100% mortality
14	4.53	100% mortality
15	1.10	EC_{12}
16	1.07	EC_{12}
17	0.75	NOEC
18	0.90	NOEC
19	5.11	100% mortality
20	4.44	100% mortality
21	6.00	100% mortality
22	1.64	EC_{50}
23	4.61	100% mortality
24	2.00	100% mortality
25	2.05	100% mortality
26	0.02	NOEC
27	1.94	EC_{95}
28	1.97	100% mortality
29	2.05	100% mortality
30	1.84	EC_{88}

Table 6. Results of the evaluation of effluent toxicity by *P. aeruginosa* bacteria.

(Table 4). A key outcome related to the model's performance was its potential applicability under real wastewater treatment conditions, where both efficiency and reliability are crucial. The strong correlation observed between predicted and experimental values indicated that the model accurately captured system behavior across diverse operational parameters. These results are consistent with previous studies reporting the efficacy of RSM in optimizing advanced organic pollutant removal techniques such as adsorption and oxidation[20,31,36].

Despite the promising statistical results obtained in this study ($R^2 = 0.9887$), it is recommended that future research undertake more rigorous validation of the model under practical application conditions, as laboratory-scale studies may overlook influential factors such as the presence of interfering substances and flow dynamics. This highlights the critical importance of strategic planning in optimizing environmental remediation processes. Therefore, future studies should focus on integrating kinetic and practical analyses with statistical methodologies to achieve a more comprehensive understanding of removal pathways and system limitations. A scatter plot of actual versus predicted values serves as a useful diagnostic tool for evaluating the performance of predictive models. As illustrated in Fig. 3, the deviations from the ideal 1:1 line, which represent potential model errors, were minimal. This close agreement between actual and predicted values indicates that systematic errors were negligible. Therefore, the model demonstrates strong validity in terms of both data normality and predictive accuracy.

The analysis of variance (ANOVA) results (Table 5) demonstrated that the initial aniline concentration and pH had statistically significant effects on the photocatalytic removal of aniline (P-value < 0.05), whereas the nanoparticle dose and contact time did not show statistically significant effects (P-value > 0.05). These findings indicate that optimizing the initial aniline concentration and solution pH is essential to improving the efficiency of the photocatalytic process. The lack of significance for nanoparticle dose and contact time may be due to the narrow range of experimental parameters or the presence of interaction effects, emphasizing the need for more comprehensive studies on the interactions among operational variables in future research. Based on the results obtained in Fig. 4a, b, c, the aniline removal efficiency increased significantly with increasing contact time, reaching a maximum of 98% at approximately 62.5 min. This trend indicated an enhanced opportunity for the interaction between aniline molecules and the active surface of the catalyst, as the prolonged contact time increased the likelihood of collisions between the molecules and reactive species such as •OH. The mechanism

underlying the effect of contact time involved the extended presence of pollutants within the reaction environment, providing more opportunities for chemical interactions between aniline and reactive species. These conditions facilitated advanced oxidation reactions, leading to the breakdown of aniline molecular bonds and more complete degradation. Specifically, increasing the contact time from 32.5 to 62.5 min resulted in an approximate 17.9% improvement in removal efficiency.

As shown in Fig. 4a, b, c, once the contact time reached 62.5 min, the aniline removal efficiency plateaued, and further increases in contact time did not result in significant improvements in process performance. This behavior is primarily attributed to the saturation of the catalyst's active surface; beyond a certain point, all available active sites become occupied, thereby limiting the catalyst's capacity to facilitate further reactions. Consequently, extending the contact time beyond this threshold does not provide additional opportunities for aniline molecules to interact with reactive species. Furthermore, the generation of reactive species such as hydroxyl •OH and other active intermediates is also affected by contact time. Increasing the duration beyond the equilibrium point can reduce the production of these species, thereby limiting the efficiency of advanced oxidation processes. This finding indicates that optimizing contact time is crucial for achieving maximum removal efficiency. Insufficient contact time leads to incomplete reactions, whereas excessive contact time can reduce process efficiency due to decreased generation of reactive species and catalyst surface saturation[17,20,37]. Therefore, to gain a more precise understanding of the role of contact time in the removal process, further studies focusing on kinetic effects, long-term system stability, and evaluation of system behavior at real-scale conditions are recommended. These findings were consistent with previous studies, including the work of Rahdar et al., who reported a maximum removal efficiency of 91.95% at a contact time of 45 min and emphasized the importance of optimizing contact time in pollutant removal processes[38]. Overall, the results of this study indicated that contact time is an influential factor in improving the efficiency of the treatment process and can serve as a scientific basis for the design and development of catalytic processes aimed at the removal of compounds such as aniline.

In this study, the aniline removal process was investigated at different pH including acidic, neutral, and alkaline. The results showed that the highest percentage of aniline removal was achieved at slightly alkaline pH (7.5). This efficiency was higher than that of acidic and neutral conditions (Fig. 4a, d, e), so that the removal efficiency under optimal conditions was reported to be 98%. According to previous studies, solution pH is one of the most effective environmental factors for the removal of pollutants by AOP processes[15,39]. One of the key factors enhancing the efficiency of AOPs is the generation of •OH, which, due to their high reactivity, can oxidize organic pollutants such as aniline into simpler compounds like carbon dioxide and water. The solution pH plays a crucial role in regulating both the formation of these radicals and the adsorption behavior of pollutants on the photocatalyst surface[20,39]. Aniline, a weak base with a pKa around 4.6, predominantly exists in its protonated ionic form ($C_6H_5NH_3^+$) under acidic conditions, which enhances its adsorption via electrostatic interactions with the catalyst surface. Meanwhile, the surface charge of TiO_2 varies with pH, with its isoelectric point (IEP) typically between 6 and 7. Below this pH range, the TiO_2 surface carries a positive charge, which can repel the positively charged protonated aniline and thus reduce absorption. However, near neutral pH values, aniline remains protonated while the TiO_2 surface charge becomes neutral or less positive, favoring stronger adsorption and, consequently, more efficient pollutant degradation. Furthermore, pH influences the generation of •OH radicals; alkaline conditions generally enhance radical formation, but excessively high pH may lead to the formation of less reactive oxidizing species, reducing overall process efficiency[20,40]. Several studies have investigated the effect of pH on the surface charge of photocatalysts such as TiO_2 and the absorption of pollutants. In this regard, Negoescu et al.[41]demonstrated that the isoelectric point of TiO_2 is approximately pH 6.5; at pH values below this point, the TiO_2 surface carries a positive charge, which leads to the repulsion of cationic aniline, whereas at pH values above this point, the surface charge becomes negative, reducing pollutant adsorption. These findings emphasize the critical role of precise pH adjustment in optimizing pollutant adsorption. Furthermore, Wang et al[42]. showed that aniline predominantly exists as the cationic species under acidic conditions, and this positively charged form enhances its adsorption on the catalyst surface through electrostatic interactions. They also noted that the surface charge of TiO_2 varies with pH; specifically, at pH values below 6, the TiO_2 surface is positively charged, potentially repelling cationic aniline, while near neutral pH, adsorption is maximized. Overall, the findings of this study, supported by previous research, emphasize the critical role of precise pH control in balancing the catalyst surface charge and pollutant speciation, thereby significantly improving the efficiency of photocatalytic degradation processes.

In this study, the removal efficiency of aniline was investigated at various initial concentrations ranging from 1 to 40 mg/L. The highest removal efficiency was observed at the lowest concentration (1 mg/L), whereas increasing the aniline concentration to 40 mg/L resulted in a decrease in removal efficiency to 85% (Fig. 4b, d, f; Table 3). This trend indicates that at lower concentrations, aniline molecules are easily adsorbed onto the surface of nanoparticles, and the generated free radicals readily react with these molecules. However, as the aniline concentration increases, the active sites on the nanoparticles become saturated, leading to intensified competition among aniline molecules for adsorption. Consequently, the accessibility of free radicals to all aniline molecules is restricted, resulting in a decline in removal efficiency[11,43]. Several studies have also reported a decrease in aniline removal efficiency at higher concentrations. For example, Anatoi et al[44]. investigated the photocatalytic oxidation of aniline using visible-light-activated titanium dioxide and found that increasing the initial aniline concentration from 0.047 to 0.80 mM caused the removal efficiency to drop significantly from 72% to 18%. This reduction was attributed to the inadequate generation of radicals necessary for complete aniline degradation Similarly, studies by Bazarafshan et al[45]. and Rahdar et al[38]. Reported that increasing the initial concentration of aniline in photocatalytic processes led to a decline in both degradation rate and removal efficiency. These findings indicate that limited catalytic reactivity and competitive adsorption among molecules are key factors restricting removal performance at higher pollutant concentrations. From a practical perspective, these results

Methods	Aniline Removal Efficiency (%)	Features	References
photochemical decomposition ($TiO_2/H_2O_2/UV$)	98.00	Laboratory conditions (pH = 7.5, NPs = 55 mg/L, contact time = 62.5 min, and initial aniline concentration = 1 mg/L,) UV irradiation	in This study
Corona Plasma	98.50	Short reaction time 7.5 min	49
Liquid Emulsion Membrane	98.53	High efficiency in membrane system	50
$CoFe_2O_4$/PAA	93.00	Oxidation using peracetic acid	51
US + H_2O_2	95.91	Optimal pH ≈ 3; reaction time: 45 min	38
Fenton process	72.57	1100 mg/L of H_2O_2, 70 mg/L of Fe^{2+} and 40 min of reaction time	37
Ozonation	93.57	Ozone dose: 22 mg/L; neutral pH; reaction time: 120 min	52
UV + CuO	90.16	Reaction time: 90 min	53
UV + ZnO	76.30	Alkaline pH; reaction time: 90 min	46
Edible Fungus residue Activated Carbon (EFAC)	86.74	Activated carbon derived from mushrooms	54

Table 7. Comparison of different aniline removal methods from aqueous solutions.

highlight the critical importance of optimizing aniline concentration in water and wastewater treatment systems to achieve maximum removal efficiency, improved catalyst utilization, and reduced operational costs.

According to the data presented in Table 4; Fig. 4c, e, f, the dosage of TiO_2 NPs significantly affected aniline removal. The results indicated an optimal concentration at 55 mg/L, where the removal efficiency reached its maximum value of 98%. However, increasing the dosage beyond this level led to a decrease of approximately 8.9% in removal efficiency, which may be attributed to particle agglomeration or light scattering effects that negatively impact photocatalytic activity. The increase in TiO_2 nanoparticle dosage enhances the number of active surface sites and promotes the generation of free electrons. This facilitates the production of reactive oxygen species (ROS), including $^{\bullet}OH$ and superoxide anions ($O_2^{\bullet-}$), which play a pivotal role in the oxidative degradation of persistent organic pollutants such as aniline. Therefore, optimizing the TiO_2 dosage is essential to maximize ROS generation and overall photocatalytic efficiency while minimizing adverse effects caused by excessive nanoparticle loading. When the nanoparticle dose exceeds the optimal concentration, the active sites on the nanoparticle surface become saturated, reducing the adsorption capacity for pollutants[38,46], Moreover, at higher dosages, titanium dioxide nanoparticles tend to aggregate, which can hinder the penetration of UV light to some particles, consequently decreasing the generation of free radicals. Ferreiro et al[47]. studied the simultaneous removal of aniline and benzothiazole from industrial wastewater using an MnO_2/GAC catalyst in a fluidized bed photocatalytic reactor. They observed that increasing the catalyst concentration up to 0.25 g/L improved removal efficiency significantly; however, further increases led to a decline in efficiency, likely due to active site saturation and reduced UV light penetration. Similarly, Basturk et al[48]. investigated the photocatalytic removal of aniline using TiO_2 nanoparticles. They reported that aniline removal efficiency increased with nanoparticle concentration up to an optimum point, beyond which active sites became saturated and the photocatalytic efficiency decreased. These findings confirm that while increasing nanoparticle dosage can enhance photocatalytic activity by providing more active sites, overdosing leads to aggregation and light shielding effects that reduce overall efficiency.

In this study, the significance of the impact coefficients associated with each variable in the aniline removal process is presented in Eq. 6. According to the results, the impact coefficients for contact time, pH, initial aniline concentration, and nanoparticle dose were calculated as −0.094837, 8.82011, −0.465425, and − 0.018612, respectively. These values indicate that among the studied variables, pH had the most significant positive influence on the removal efficiency, while nanoparticle dose had the least effect. Therefore, based on these findings, pH can be considered a key factor in the photocatalytic degradation of aniline. In this study, the photocatalytic process demonstrated a satisfactory performance in aniline removal, comparable to the efficiencies reported for various advanced water treatment methods in previous studies (Table 7). For example, corona plasma technology achieved 98.5% efficiency[49], the liquid emulsion membrane process reached up to 98.53%[50], and advanced oxidation systems such as $CoFe_2O_4$/PAA showed efficiencies of up to 93%[51]. Furthermore, compared to more conventional methods such as ozonation (93.57%)[52] and UV/ZnO (76.3%)[46], the proposed method demonstrated higher effectiveness. These findings indicate the strong potential of the investigated photocatalytic process for the effective degradation of persistent pollutants.

Given the critical importance of environmental protection and public health, thorough evaluation of potential byproducts in wastewater treatment processes, including photocatalysis, is essential. Although photocatalytic processes effectively degrade persistent pollutants, the formation of toxic intermediate compounds during treatment remains a significant concern. These intermediates, if not adequately monitored, may pose environmental and health risks. Therefore, comprehensive toxicity assessments of treated effluents are crucial to ensure their safety prior to discharge into natural water bodies[27,28,31,48]. The results of the toxicity evaluation of aniline on *P. aeruginosa* are presented in Table 6. Accordingly, the EC_{50} and 100% mortality values were determined to be 1.64 and 1.97 mg/L, respectively. The obtained data demonstrated the significant toxicity of the aniline-containing effluent and its detrimental effect on the survival of *P. aeruginosa*. Although no mortality was observed at an aniline concentration of 0.91 mg/L, both the EC_{50} and 100% mortality were recorded at relatively low aniline concentrations. Therefore, to ensure environmental safety, the aniline concentration in the effluent should not exceed 0.91 mg/L. Previous studies have shown that *P. aeruginosa* is capable of degrading

aniline under certain conditions. Nevertheless, at higher concentrations, its biodegradation capacity diminishes, leading to persistent toxicity in the effluent. This is consistent with the present findings, where residual toxicity was observed despite the biodegradation potential[55]. Similar to the present study, Toolabi et al.[20] employed the AB reduction test to assess bacterial toxicity in effluent from a TiO_2/Fe_2O_4/UV photocatalytic process. Their findings confirmed the sensitivity and reliability of the AB assay for detecting toxic effects in treated wastewater. One limitation of the present study is the use of a single bacterial strain, which may not fully detect or respond to the entire range of pollutants present in industrial effluents. Therefore, it is recommended that future research employ a combination of biological and chemical methods to improve the accuracy of toxicity assessments of treated effluent.

Conclusion

In this study, the TiO_2/H_2O_2/UV oxidation process was effectively evaluated for the optimization of aniline removal from aqueous solutions. Among the examined variables, pH was identified as the most influential factor in aniline degradation. The high coefficient of determination ($R^2 = 0.9887$) confirmed the accuracy and reliability of the quadratic model. Under optimal conditions, the TiO_2 photocatalytic process, in the presence of H_2O_2 and UV irradiation, was able to remove up to 98% of aniline from aqueous solution, indicating acceptable efficiency at the laboratory scale. Furthermore, the bacterial toxicity of the treated effluent was assessed using the AB reduction assay, which is recognized as a reliable method. According to the results, the EC_{50} and NOEC values were determined to be 1.64 and 0.91 mg/L, respectively, indicating a significant reduction in aniline toxicity following the photocatalytic treatment process.

Although this process demonstrated high efficiency in aniline removal, it also exhibited certain limitations, including the absence of a comprehensive evaluation of by-products generated during aniline degradation and the high energy consumption associated with UV irradiation observed in the experiments. To improve performance and expand the applicability of this process for aniline treatment, future studies are recommended to conduct detailed investigations into the degradation pathways and identification of intermediate by-products. From a practical perspective, a thorough assessment of the scale-up potential of the TiO_2/H_2O_2/UV process for treating real industrial wastewater is necessary to support its industrial application. Additionally, an in-depth analysis of energy consumption and economic feasibility is essential to evaluate the practical viability of this process at larger scales.

Data availability

All data generated or analyzed during this study are included in this published article.

Received: 22 July 2025; Accepted: 14 November 2025
Published online: 23 November 2025

References

1. Natarajan, S., Bajaj, H. C. & Tayade, R. J. Recent advances based on the synergetic effect of adsorption for removal of dyes from waste water using photocatalytic process. *J. Environ. Sci.* **65**, 201–222 (2018).
2. Lincho, J., Zaleska-Medynska, A., Martins, R. C. & Gomes, J. Nanostructured photocatalysts for the abatement of contaminants by photocatalysis and photocatalytic ozonation: an overview. *Sci. Total Environ.* **837**, 155776 (2022).
3. Liu, H., Wang, C. & Wang, G. Photocatalytic advanced oxidation processes for water treatment: recent advances and perspective. *Chemistry–An Asian J.* **15**, 3239–3253 (2020).
4. Pirsaheb, M. et al. Photocatalytic degradation of aniline from aqueous solutions under sunlight illumination using immobilized cr: ZnO nanoparticles. *Sci. Rep.* **7**, 1473 (2017).
5. Ahmadi, S., Mostafapour, F. & Bazrafshan, E. Removal of aniline from aqueous solutions by coagulation/flocculation–flotation. *Chem. Sci. Int. J.* **1**, 1–10 (2017).
6. Xue, G. et al. Comparison of aniline removal by UV/CaO2 and UV/H2O2: degradation kinetics and mechanism. *Chemosphere* **255**, 126983 (2020).
7. Liao, Y., Meng, X., Shi, L. & Liu, N. NH4F modified β zeolite for aniline condensation to diphenylamine and its catalytic mechanism. *Catal Commun.* **175**, 106624 (2023).
8. Xue, G. et al. Simultaneous removal of aniline, antimony and chromium by ZVI coupled with H2O2: implication for textile wastewater treatment. *J. Hazard. Mater.* **368**, 840–848 (2019).
9. Ahmadi, S. & Igwegbe, C. A. Adsorptive removal of phenol and aniline by modified bentonite: adsorption isotherm and kinetics study. *Appl. Water Sci.* **8**, 1–8 (2018).
10. Chaturvedi, N. K. & Katoch, S. S. Remedial technologies for aniline and aniline derivatives elimination from wastewater. *J. health pollut.* **10**, 1–11 (2020).
11. Zhou, Y., Tuo, H. U. Z. & Yang, Z. Photocatalytic degradation of aniline using supported TiO2/Charcoal composite. *Asian J. Chem.* **26**, 5579–5582 (2014).
12. Chaturvedi, N. Comparison of available treatment techniques for hazardous aniline–based organic contaminants. *Appl. Water Sci.* **12**, 173 (2022).
13. Jia, Z., Yang, Y., Yang, C. & Wang, D. Magnetic γ-Fe2O3/ZnO@CNTs synthesized by a green precipitation method for the degradation of aniline through photocatalysis coupling catalytic ozonation. *Appl. Surf. Sci.* **659**, 159866 (2024).
14. Shang, H., Xia, Y., Zhou, Y., Liu, G. & Hu, X. Removal of aniline from wastewater by electro-polymerization with superior energy efficiency. *Environ. Res.* **190**, 109931 (2020).
15. Mohamadiyan, J. et al. Aniline degradation using advanced oxidation process by UV/Peroxy disulfate from aqueous solution. *Int. J. Eng.* **30**, 684–690 (2017).
16. Li, X. et al. Coupled treatment of aniline and phenol in water by electrochemical copolymerization. *Water Sci. Technolog.* **90**, 1–13 (2024).
17. Nakhostin Panahi, P. & Nikoo, A. Aniline removal from polluted water with photocatalytic oxidation process by zinc oxide loaded with carbon. *J. Appl. Res. Chemisry.* **15**, 1–11 (2021).
18. Khan, Z. U. H. et al. Removal of organic pollutants through hydroxyl radical-based advanced oxidation processes. *Ecotoxicol. Environ. Saf.* **267**, 1–15 (2023).

19. Shahrezaei, F., Mansouri, Y., Zinatizadeh, A. A. L. & Akhbari, A. Photocatalytic Degradation of Aniline Using TiO2 Nanoparticles in a Vertical Circulating Photocatalytic Reactor. *Int. J. Photoenergy*. **2012**, 8 – 1 (2012).
20. Toolabi, A. et al. Optimizing the photocatalytic process of removing Diazinon pesticide from aqueous solutions and effluent toxicity assessment via a response surface methodology approach. *Rend. Lincei Scienze Fis. E Naturali*. **30**, 155–165 (2019).
21. Sharma, R. & Prakash, J. TiO2 nanomaterials: Synthesis, Properties, Modifications, and applications. *Eng. Mater*, 1–25 (2025).
22. Mayahi, B., Arbabi, M. & Hemati, S. Optimization of UV/H2O2/Fe3O4 process to remove aniline from aqueous solutions using central composite methodology. *Desalination Water Treat.* **136**, 252–258 (2018).
23. Yabalak, E., Topaloğlu, I. & Gizir, A. M. Multi response central composite design of the mineralization and removal of aniline by subcritical water oxidation method. *Int. J. Industrial Chem.* **10**, 97–105 (2019).
24. Longhin, E. M., Yamani, N. E., Rundén-Pran, E. & Dusinska, M. The Alamar blue assay in the context of safety testing of nanomaterials. *Front. Toxicol.* **4**, 981701 (2022).
25. Zare, M. et al. Simplification and sensitivity study of Alamar blue bioassay for toxicity assessment in liquid media. *Desalination Water Treat.* **136**, 252–258 (2016).
26. Al-Nasiry, S., Geusens, N., Hanssens, M., Luyten, C. & Pijnenborg, R. The use of Alamar blue assay for quantitative analysis of viability, migration and invasion of choriocarcinoma cells. *Hum. Reprod.* **22**, 1304–1309 (2007).
27. Zare, M. et al. Resazurin reduction assay, a useful tool for assessment of heavy metal toxicity in acidic conditions. *Environ. Monit. Assess.* **187**, 1–11 (2015).
28. Toolabi, A. et al. Optimization of photochemical decomposition Acetamiprid pesticide from aqueous solutions and effluent toxicity assessment by Pseudomonas aeruginosa BCRC using response surface methodology. *Amb Express*. **7**, 1–12 (2017).
29. Mahon, R. C. & Lehman, C. D. *Textbook of Diagnostic Microbiology, 1154* (elsevier, 2022).
30. Girma, A. & Aemiro, A. The Bacterial Profile and Antimicrobial Susceptibility Patterns of Urinary Tract Infection Patients at Pawe General Hospital, Northwest Ethiopia. *Scientifica*, 1–8 (2022).
31. Toolabi, A. et al. Modeling photocatalytic degradation of Diazinon from aqueous solutions and effluent toxicity risk assessment using Escherichia coli LMG 15862. *AMB Express*. **8**, 1–13 (2018).
32. Lotfigolsefidi, F., MDavoudi, Sarkhosh, M. & Bonyadi, Z. Removal of microplastics by algal biomass from aqueous solutions: performance, optimization, and modeling. *Sci. Rep.* **15**, 501 (2025).
33. Diebold, U. The surface science of titanium dioxide. *Surf. Sci. Rep.* **48**, 53–229 (2003).
34. Nematov, D. Titanium dioxide and photocatalysis: A detailed overview of the Synthesis, Applications, Challenges, advances and prospects for sustainable development. *J. Mod. Green. Energy*. **3**, 1–32 (2024).
35. Sharma, R. & Prakash, J. *In Titanium Dioxide-Based Multifunctional Hybrid Nanomaterials: Application on Health, Energy and Environment (eds Jai Prakash, Junghyun Cho, Olim Ruzimuradov, & Dong Fang) 1–25* (Springer Nature Switzerland, 2025).
36. Ali, I., Asim, M. & Khan, T. A. Low cost adsorbents for the removal of organic pollutants from wastewater. *J. Environ. Manage.* **113**, 170–183 (2018).
37. Mousavi, S., Farrokhi, F., Kianirad, N. & Falahi, F. Degradation of aniline from aqueous solution by Fenton process: modeling and optimization. *Desalination Water Treat.* **125**, 68–74 (2018).
38. Rahdar, S., Igwegbe, C., Ghasemi, M. & Ahmadi, S. Degradation of aniline by the combined process of ultrasound and hydrogen peroxide (US/H2O2). *MethodsX* **6**, 492–499 (2019).
39. Gawad, H., Ebrahiem, E., Ghaly, M., Afify, A. & Mohamed, R. An application of advanced oxidation process on industrial crude oily wastewater treatment. *Sci. Rep.* **13**, 3420 (2023).
40. Zhu, X., Castleberry, S., Nanny, M. & Butler, E. Effects of pH and catalyst concentration on photocatalytic oxidation of aqueous ammonia and nitrite in titanium dioxide suspensions. *Environ. Sci. Technol.* **39**, 3784–3791 (2005).
41. Negoescu, D. et al. Active Ag-, Fe-, and AC-Modified TiO2 mesoporous photocatalysts for anionic and cationic dye degradation. *Catalysts* **15**, 479 (2025).
42. Wang, X., Zhang, X. & Li, Z. Adsorption and photocatalytic degradation of aniline on TiO_2 surface: effects of pH and surface charge. *Appl. Surf. Sci.* **427**, 575–583 (2018).
43. Xu, J., Jia, H., Ma, H., Tian, C. & Zhu, C. Salinity relief aniline induced oxidative stress in Suaeda salsa: activities of antioxidative enzyme and EPR measurements. *Ecotoxicol. Environ. Saf.* **205**, 111293 (2020).
44. Anotai, J., AJevprasesphant, Lin, Y. M. & Lu, M. C. Oxidation of Aniline by Titanium Dioxide Activated with Visible Light. *Separation and Purification Technology* **84,** 132-137 (2012).
45. Bazrafshan, E., Noorzaei, S. & KordMostafapour, F. Photocatalytic degradation of aniline in aqueous solutions using magnesium oxide nanoparticles. *J. Mazandaran Univ. Med. Sci.* **26**, 126–136 (2016).
46. fard, E. D., Jafari, A. J., Kalantari, R. R., Gholami, M. & Esrafili, A. Photocatalytic removal of aniline from synthetic wastewater using ZnO nanoparticle under ultraviolet irradiation. *Iran. J. Health Environ.* **5**, 168–177 (2012).
47. Ferreiro, C., Villota, N., Lombraña, J. & Rivero, M. J. An efficient catalytic process for the treatment of genotoxic aniline wastewater using a new granular activated carbon-supported titanium dioxide composite. *J. Clean. Prod.* **228**, 1282–1295 (2019).
48. Basturk, E., Işık, M. & Karatas, M. Removal of aniline (Methylene Blue) and Azo (Reactive red 198) dyes by photocatalysis via nano TiO2. *Desalin. Water Treat.* **143**, 306–313 (2019).
49. Li, Y. et al. Degradation of aniline in water with gaseous streamer Corona plasma. *R Soc. Open. Sci.* **8**, 202314 (2025).
50. Chaturvedi, N. & Katoch, S. Remedial technologies for aniline and aniline derivatives elimination from wastewater. *J. Health Pollution*. **25**, 200302 (2020).
51. Gao, J., Yang, P., Zhu, M., Zhou, H. & Pan, S. Advanced degradation of aniline in secondary effluent from a chemical industry park by Cobalt Ferrite/Peracetic acid system. *Catalysts* **15**, 1–17 (2025).
52. Jing, Z., Cao, S., Yu, T. & Hu, J. Degradation characteristics of aniline with ozonation and subsequent treatment analysis. *J. Chem.* **4**, 1–6 (2015).
53. Norzaee, S., Djahed, B., Khaksefidi, R. & Mostafapour, F. K. Photocatalytic degradation of aniline in water using CuO nanoparticles. *AQUA - Water Infrastructure Ecosyst. Soc.* **66**, 2017104 (2017).
54. Li, H. et al. High-efficiency adsorption and regeneration of methylene blue and aniline onto activated carbon from waste edible fungus residue and its possible mechanism. *RSC Adv.* **10**, 14262–14273 (2020).
55. Mohlam, F., Bakeer, W., El-Gebaly, E. & Amin, M. Molecular characterization of aniline biodegradation by some bacterial isolates having unexpressed catechol 2,3-Dioxygenase gene. *J. Pure Appl. Microbiol.* **12**, 2027–2039 (2018).

Acknowledgements

The authors would like to thank the financial support provided by the Lorestan University of Medical Sciences, Iran.

Author contributions

M.GH: Writing, editing. M.H: Writing, original draft. F.A: Editing, Investigation. B.K: Inves-tigation, Methodology. A.T: Writing, review, editing, Supervision.

Funding
This study was financially supported (No. 1397-1-99-3323, Ethics approval: IR.LUMS.REC.1402.214) by Lorestan University of Medical Sciences (Iran).

Declarations

Competing interests
The authors declare no competing interests.

Additional information
Correspondence and requests for materials should be addressed to A.T.

Reprints and permissions information is available at www.nature.com/reprints.

Publisher's note Springer Nature remains neutral with regard to jurisdictional claims in published maps and institutional affiliations.